Pharmacophore modelling and 3D-QSAR studies on antithrombotic activity of biphenyl analogues

Aparna N. Jadhav[1,*], Radha C. Dash[1], Raj R. Hirwani[1] and Malik Z. Abdin[2]

[1]Council of Scientific and Industrial Research – Unit for Research and Development of Information Products, 85/1, Jopasana, Paud Road, Kothrud, Pune 411 038, India
[2]Department of Biotechnology, Faculty of Science, Jamia Hamdard, New Delhi 110 062, India

Thrombin regulates blood coagulation and has a central role in haemostasis. Antithrombotic compounds such as biphenyl derivatives are known to target thrombin and can significantly treat thrombosis-related disorders. In this communication we describe *in silico* methods such as generation of common pharmacophore hypothesis and 3D-QSAR model, based on the structural features of biphenyl derivatives. The best pharmacophore hypothesis generated consists of three features, namely two aromatic rings (R), two hydrogen donors (D) and one positive ionizable group (P). To validate common pharmacophore and 3D-QSAR models, biphenyl derivatives were docked against the available 3D structure of thrombin (PDB: 2C8W), which gave the best scoring and interactions with compound 4. The statistically validated 3D-QSAR illustrates good predictability values and root mean square error. Our finding helps identify the structure–activity relationship of biphenyl derivatives against thrombin.

Keywords: Antithrombin, biphenyl derivatives, pharmacophore, thrombin

HAEMOSTASIS is the mechanism of blood loss control in the event of vascular injury. It triggers formation of a platelet plug, thrombin and fibrin clot through blood coagulation to arrest bleeding. A minor imbalance in such highly regulated haemostatic system could lead to haemorrhagic disorders or thrombosis[1,2]. During thrombosis, the blood clots are formed inside the blood vessel obstructing blood flow through the circulatory system. To avoid such blood clots, plasma antithrombin-III factor inhibits thrombin from clot formation. Thrombin, a serine protease, plays a central role in regulating blood coagulation by clot formation and inhibition. It activates fibrinogen to fibrin formation and other glycoprotein factors such as FV[3], FVIII[4], FXI[5] and FXIII[6] which are essential components of the blood coagulation cascade. Inhibition of thrombin prevents the generation of these factors and eventually blood coagulation; hence is the best target for interference[7].

*For correspondence. (e-mail: aparna_jadhav@urdip.res.in)

Presently, oral anticoagulants and heparins are the only available therapy for treatment of the major thrombotic disorders[8,9]. Development of newer anticoagulants with single target inhibition has gained importance, as it offers improved efficiency and safety compared to existing therapies[10]. Thrombin being multifunctional has the ability to interact with distinct ligands and consequently becomes the prime target for anticoagulants[11–13]. Earlier research had shown that inhibition of thrombin by diverse potent compounds could provide invaluable drugs to the treatment of disorders related to thrombosis[14]. Biphenyl compounds are useful in the treatment or prevention of thrombotic and cardiovascular disorders[15]. Recently synthesized compounds such as 4′-(6,7-dihydro-4H-thieno-[3,2-c]pyridin-5-ylmethyl)-biphenyl-2-carboxylic acid (**a**) (Figure 1) derivatives are promising antithrombotic agents[16]. 5-[2′-(1H-tetrazol-5-yl)-biphenyl-4-ylmethyl]-4,5,6,7-tetrahydro-thieno[3,2-c]pyridines (**b**) (Figure 1) have been reported to exhibit good *in vivo* antithrombotic activity compared to Clopidogrel[17]. (2-methoxy-4-biphenyl)acetylene is used to treat vascular thrombosis in warm-blooded animal[18].

In silico design and development has helped prompt identification of drug-like chemical entities for varied ailments. To comprehend therapeutic significance of thrombin inhibitors, here we propose 3D quantitative structure–activity relationship analysis (3D-QSAR) on the series of biphenyl compounds reported to have antithrombin activity[19]. These compounds have common scaffold and their biological assays performed under a single experiment, thus were used for the purpose of 3D-QSAR modelling.

Quantitative pharmacophore and 3D-QSAR model generation methods help evaluate protein–ligand interactions, which are widely used for lead optimization[20]. In the present study, we have developed quantitative pharmacophore model based on previously published biphenyl compound dataset[19]. Based on the key structural features of the compounds, pharmacophoric characteristics are developed employing PHASE module of Schrödinger molecular modelling software[21]. Atom-based 3D-QSAR analysis was performed in order to analyse the structure–activity relationship of these thrombin inhibitors. Further,

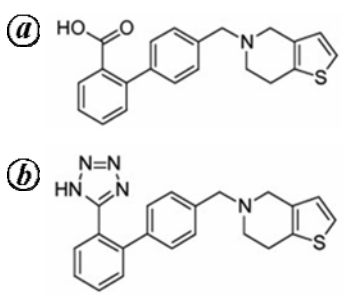

Figure 1. Previously reported biphenyl derivates having antithrombotic activity.

Table 1. Dataset analysed with experimental and predicted activities

Compound number	*R*th position	IC_{50} (nM)	Experimental 1/log IC_{50}	PLS factor	Predicted 1/log IC_{50}	QSAR set	Pharmaset	Fitness value
1	H	64	–2.806	4	–2.7	Training	Inactive	2.96
2	OH	50	–2.699	4	–2.7	Test		2.98
3	OCH3	14.87	–2.172	4	–2.22	Training	Active	2.98
4	Prop-1-ene	9.4	–1.973	4	–2.13	Test	Active	2.96
5	Prop-1-yne	50.24	–2.701	4	–2.34	Test		2.98
6	Prop-1-en-2-yl	17.9	–2.253	4	–2.21	Training		2.97
7	Buta-1,2-diene	27.96	–2.447	4	–2.27	Test		2.94
8	But-2-yne	50	–2.699	4	–2.84	Training		2.83
9	(Z)-Pent-2-ene	4.88	–1.688	4	–1.81	Training	Active	2.97
10	2-Methylpent-2-ene	12.98	–2.113	4	–1.98	Training	Active	2.91
11	Prop-2-en-1-ol-3-yl	22.73	–2.357	4	–2.39	Training		2.9
12	2-Methylprop-2-en-1-ol	39.7	–2.599	4	–2.56	Training		2.85
13	(E)-Pent-3-en-1-ol	56.22	–2.75	4	–2.72	Training	Inactive	2.9
14	Pent-3-yn-1-ol	17.9	–2.253	4	–2.23	Training		2.92
15	Propane-1,2-diol	50	–2.699	4	–2.85	Test		2.95
16	Toluene	11.82	–2.073	4	–2.08	Training	Active	2.88
17	Ethylbenzene	8.51	–1.93	4	–2.06	Training	Active	2.86
18	4-Methylpyridine	35.39	–2.549	4	–2.52	Training		2.87
19	3-Methylpyridine	50	–2.699	4	–2.62	Training		2.9
20	2-Methylthiophene	8.02	–1.904	4	–1.94	Training	Active	2.9
21	3-Methylthiophene	14.99	–2.176	4	–2.12	Training	Active	2.89
22	2-Methylfuran	14.67	–2.166	4	–2.25	Training	Active	2.92
23	2-Methyl-1H-pyrrole	19.88	–2.298	4	–2.3	Training		2.7
24	1,2-Dimethyl-1H-pyrrole	86.86	–2.939	4	–3.01	Training	Inactive	2.87
25	2-Methylthiazole	70.4	–2.848	4	–2.77	Training	Inactive	2.92
26	2-Ethylthiophene	42.12	–2.624	4	–2.63	Test		2.84
27	(3-Methylthiophen-2-yl)methanol	50	–2.699	4	–2.62	Training		2.9
28	(2-Methylthiophen-3-yl)methanol	50	–2.699	4	–2.74	Test		2.9
29	(4-Methylthiophen-3-yl)methanol	63.1	–2.8	4	–2.84	Training	Inactive	2.88
30	(4-Methylthiophen-3-yl)methanamine	110.48	–3.043	4	–2.95	Training	Inactive	2.89
31	(2-Methylfuran-3-yl)methanol	50	–2.699	4	–2.66	Training		2.87
32	3-Methylfuran	16.07	–2.206	4	–2.24	Test		2.92
33	3-Azido-4-methylthiophene	156.8	–3.195	4	–3.34	Training	Inactive	2.84
34	Butane	39.57	–2.597	4	–2.5	Training		2.93
35	Ethyl	12.3	–2.09	4	–2.22	Test	Active	3
36	But-1-ene	19.17	–2.283	4	–2.37	Training		2.95

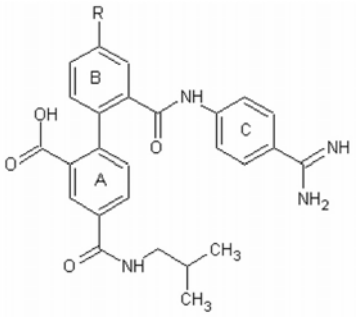

Figure 2. General structure of the biphenyl compounds.

the compounds were docked against the 3D structure of thrombin to evaluate the developed pharmacophore and 3D-QSAR models.

A set of 36 synthetic biphenyl derivatives (Table 1) with well-defined antithrombin activity was used for the QSAR analysis. *In vitro* inhibitory concentrations (IC_{50}) of the compounds against thrombin were converted into pIC_{50}(1/log IC_{50}) values. These values were used as biological activity parameter and as dependent variables in the QSAR calculations. One core molecule as shown in Figure 2 containing biphenyl ring as basic structure, represents all the 36 molecules which were considered for the analysis. The core molecule contains three aromatic rings, namely A, B and C. The aromatic rings A and C are fixed, while substitution at the 4-position of aromatic ring B was taken into consideration to generate common pharmacophoric hypothesis.

Generation of pharmacophore hypothesis and atom-based 3D-QSAR studies were accomplished using PHASE 3.0 module of Schrödinger molecular modelling tool[21]. PHASE is convenient for common pharmacophore identification and assessment, 3D-QSAR model development, 3D database creation and searching[22].

Build and Maestro modules were used to create unique low-energy 3D structures of the ligands. These structures were minimized by applying default universal force field within Maestro. Maximum of 1000 conformers were

generated for each structure using minimization of 100 steps. Conformational space of all the molecules was explored using Monte-Carlo Multiple Minimum (MCMM)/ Low Mode (LMOD) combinations[23]. Each minimized conformer was filtered through a relative energy gap of 10 kJ mol^{-1} and a minimum atom deviation of 2.00 Å to eliminate inessential conformers. A systematic exploration about rotatable bonds is performed; it calculates the associated conformational energies, retaining only the most reasonable conformations. A high-dimensional, tree-based partitioning algorithm is applied, which exhaustively identifies spatial arrangements of functional groups that are common and essential to the biological activity of the active set of high-affinity ligands. It helps to quickly locate plausible pharmacophores from different conformations. These conformations were placed in multi-dimensional boxes; each box represents a common pharmacophore, only if it contains a sufficient number of active ligands. PHASE determines how molecular structure affects drug activity by dividing the space into a fine cubic grid, encoding atom-type occupation as numerical information and performing a partial least squares (PLS) regression, which results in the prediction of a significant pharmacophore[21]. Based on the varied structural features of the ligands and the significant pharmacophore identified, a predictive atom-based 3D-QSAR model is developed. This model helps characterize the structure–activity relationship of the ligands and the target.

In this ligand-based pharmacophore modelling, active compounds were considered for generation of common 3D pharmacophore hypothesis. The entire dataset was divided into active and inactive pharmasets according to manual definition of threshold. While defining these pharmasets, compounds having threshold value $1/\log IC_{50} > -2.176$ were designated as active and those with $1/\log IC_{50} < -2.750$ as inactive (Table 1). PHASE provides default pharmacophoric features such as hydrogen bond acceptor (A), hydrogen bond donor (D), hydrophobic group (H), negative ionizable centres (N), positive ionizable centres (P) and aromatic ring (R). These default features were used for development of pharmacophore sites[24].

Common pharmacophore hypothesis was derived from all conformations of the active ligand, which have identical set of features and the same spatial arrangement keeping a minimum inter-site distance of 2.0 Å in a final box size of 1.0 Å. Scoring function was used to analyse the hypothesis, by setting the root mean square deviation (RMSD) value below 1.2 with default options for distance tolerance. Ideal alignment of the active ligands from each box was determined by evaluating common pharmacophore hypothesis and scoring function. Various hypotheses created were ranked based on survival values for both active and inactive molecules. Based on the ranks further study was carried out to get an appropriate hypothesis.

A detailed analysis of ligand–receptor interactions was carried out by atom-based 3D-QSAR modelling. Initially the dataset was divided into training set (75%) and test set (25%) in a random manner (Table 1). Training set compounds were selected such that they represent a varied range of structural features and biological activities; whereas in the test set moderately active and less active compounds were included to spread out the range of activities[25]. Generated pharmacophore-based alignment of the 3D structures of molecules was used to derive a predictive atom-based 3D-QSAR model. The 3D-QSAR model was generated for the selected hypothesis using training set containing 29 compounds using a grid spacing of 1.0 Å. The best 3D-QSAR model was validated by predicting activities of the test set of seven compounds. The overall performance of various pharmacophore models with respect to different statistical parameters such as R^2, Q^2, Pearson-R, SD, RMSE and F-value was used for the selection of the best QSAR model. The PLS regression method was performed using PHASE with a maximum of $N/5$ PLS factors (N is the number of ligands in the training set). The predicted $1/\log IC_{50}$ at 4th PLS which is found to have good statistics, is shown in Table 2.

For docking of thrombin and biphenyl compounds, crystal structure of human thrombin was obtained from the Protein Data Bank (PDB code: 2C8W), having resolution of 1.6 Å. The docking studies were performed using GLIDE module of Schrödinger[26]. It performs grid-based ligand docking with energetics and searches for favourable interactions between one or more typically small ligand molecules and a typically larger receptor molecule, usually a protein[27]. GLIDE provides three different levels of docking precision: HTVS – high-throughput virtual screening; SP – standard precision and XP – extra precision. The protein was optimized from its raw state using Protein Preparation Wizard with RMSD of 0.3 Å and applying the OPLS_2005 force field for minimization in the Schrödinger package[28]. Receptor grid generation was accomplished using GLIDE. Grid file for receptor was generated employing co-crystallized ligand of biphenyl

Table 2. Statistical values for 3D-QSAR model generated by PLS

Training set	Test set
$m = 4$	
$n = 29$	$nT = 7$
$R^2 = 0.9531$	$Q^2 = 0.6664$
SD = 0.089	RMSE = 0.1605
$F = 111.7$	Pearson-R = 0.8213
P = 2.803e-014	

m is the number of PLS factors in the model; n the number of molecules in the training set; nT the number of molecules in test set; R^2 the coefficient of determination; $Q^2 = R^2$ for the test set; SD is the standard deviation of regression; RMSE is the root-mean squared error; F is the variance ratio; P is the statistical significance and Pearson-R is the Pearson correlation coefficient.

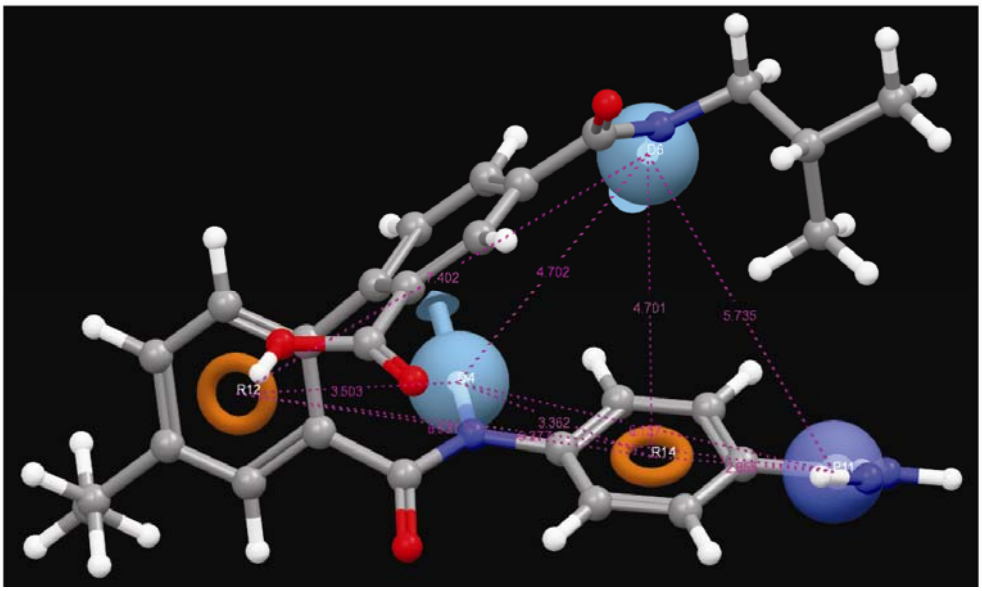

Figure 3. Generated pharmacophore model DDPRR aligned on the best-fit compound **35** (greenish blue sphere: D; blue sphere: P; orange torus: R).

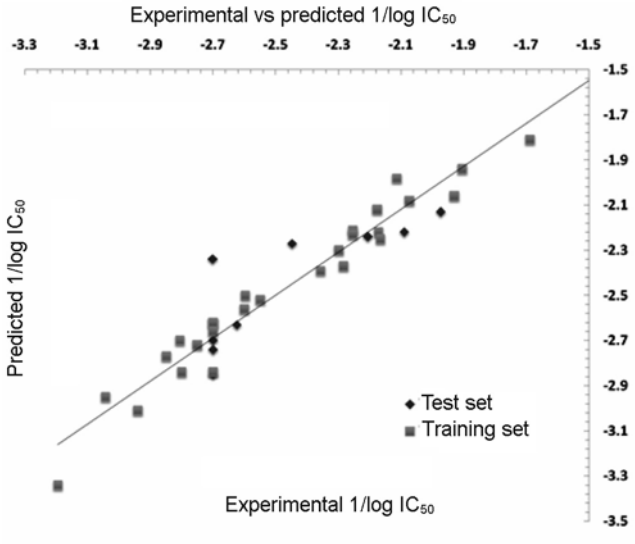

Figure 4. Scattered plot for predicted 1/log IC_{50} against experimental 1/log IC_{50} for training and test set compounds.

analogue. An extra precision (XP) flexible GLIDE docking simulation was carried out by performing 1000 poses per docking run, yielding an output of five poses per ligand with an RMSD deviation of less than 0.5 Å. Best pose of the docking interaction was selected on the basis of Glide score. This score is based on favourable and unfavourable interactions of ligands with amino acids in the active site. Maestro 9.0 interface was used to visualize and analyse the docking interactions.

The aim of the present study is to comprehend the 3D structural features of biphenyl derivatives as thrombin inhibitors, by generating 3D pharmacophores and quantifing these features by building atom-based 3D-QSAR model. PHASE module of Schrödinger suite was used for pharmacophore modelling and QSAR studies. The hypothesis generated gives insight into the relative binding of the ligands to the active site of thrombin. Conformations suggested by the hypothesis were used to build the 3D-QSAR model, which helps identify all aspects of molecular structures required for thrombin inhibitory activity.

In the present study, 10 compounds representing the active pharmaset were used to develop the pharmacophore model. Forty-five different pharmacophore hypothesis were generated using a tree-based partition algorithm, out of which a five-point pharmacophore hypotheses having two H-bond donors (D), two aromatic rings (R) and one positive ionizable group (P) was found to be the best with the highest survival active score of 3.738 and survival inactive score of 2.654. According to the core structure shown in Figure 2, A and C act as aromatic rings in generating common pharmacophore model. As in Figure 3, the whole pharmacophore feature is divided into two domains. One contains H-bond donor amide group (D4) which is linked between the two aromatic hypotheses (R12 and R14) and another domain having amide group attached to para position with respect to positive ionizable group hypothesis (P11). The five-point pharmacophore model DDPRR with its inter-site distances is shown in Figure 3.

Further to carry out atom-based 3D-QSAR analysis, all the 36 compounds were aligned on the generated pharmacophore model and randomly divided into a training set (29 molecules) and a test set (7 molecules). The PHASE descriptors served as independent variables and the activity

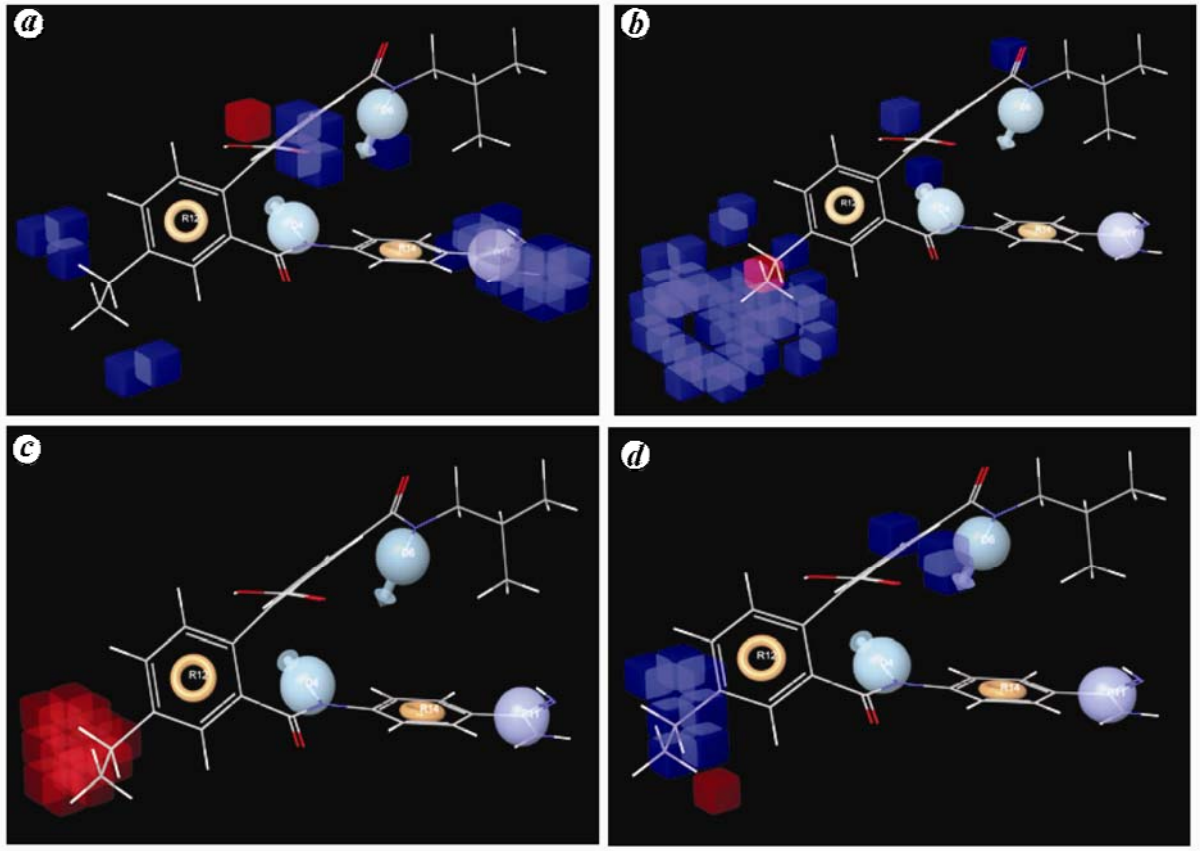

Figure 5. 3D-QSAR visualization for compound **4**. ***a***, H-bond donor; ***b***, Hydrophobicity; ***c***, Electron negative; ***d***, Electron-withdrawing features. (Blue cubes: favourable influence on activity; red cubes: unfavourable influence on activity.)

Table 3. Docking scores of active pharmaset

Compound	Docking score
4	–9.6583
16	–9.0524
20	–8.7154
9	–8.6431
22	–8.4151
3	–8.3327
35	–8.2544
10	–7.3167
17	–6.7743
21	–4.0105

values as dependent variables in deducing 3D-QSAR models by PLS regression analysis method. The PLS described in PHASE has five PLS factors out of which the fourth factor is found to be dominant. The predictive ability of the generated 3D-QSAR model was evaluated by applying it on the test set molecules. The values of SD, R^2, F and P were used to evaluate the training set predictions, whereas the values of RMSE, Q^2 and Pearson-R were used for the test set predictions. The training set achieved the highest value of $R^2 = 0.9531$, $F = 111.7$ and the lowest value of SD = 0.089 and P = 2.803e-014. The test set achieved the highest value of $Q^2 = 0.6664$, Pearson-$R = 0.8213$ and the lowest value of RMSE = 0.1605. The correlation graph between predicted and actual 1/log IC_{50} of both training and test set is depicted in Figure 4.

In order to gain additional insights into the nature of interactions of the ligands with thrombin receptor, we visualized and analysed the 3D-QSAR models based on active reference compound **4** using hydrogen-bond donor, hydrophobicity, electron-negative and electron-withdrawing features. The volume occlusion maps obtained from 3D-QSAR study (Figure 5) are useful to identify the importance of these properties with respect to the biological activity of the ligands. In these maps, blue cube areas indicate favourable regions and red cube areas indicate unfavourable regions for inhibitory activity.

The volume occlusion map of H-bond donor (Figure 5 *a*) shows very less blue blocks near the 4-position of the aromatic ring hypothesis (R12). This explains that in these biphenyl compounds, the absence of H-bond donor groups increases biological activity. Representative examples are compounds such as **4**, **5**, **9**, **10** and **16**, which show increase in thrombin inhibitory activity. While compounds such as **2**, **11–15**, which have hydrogen-bond donor groups, i.e. hydroxy group at 4-position of the aromatic ring hypothesis (R12), show decrease in biological

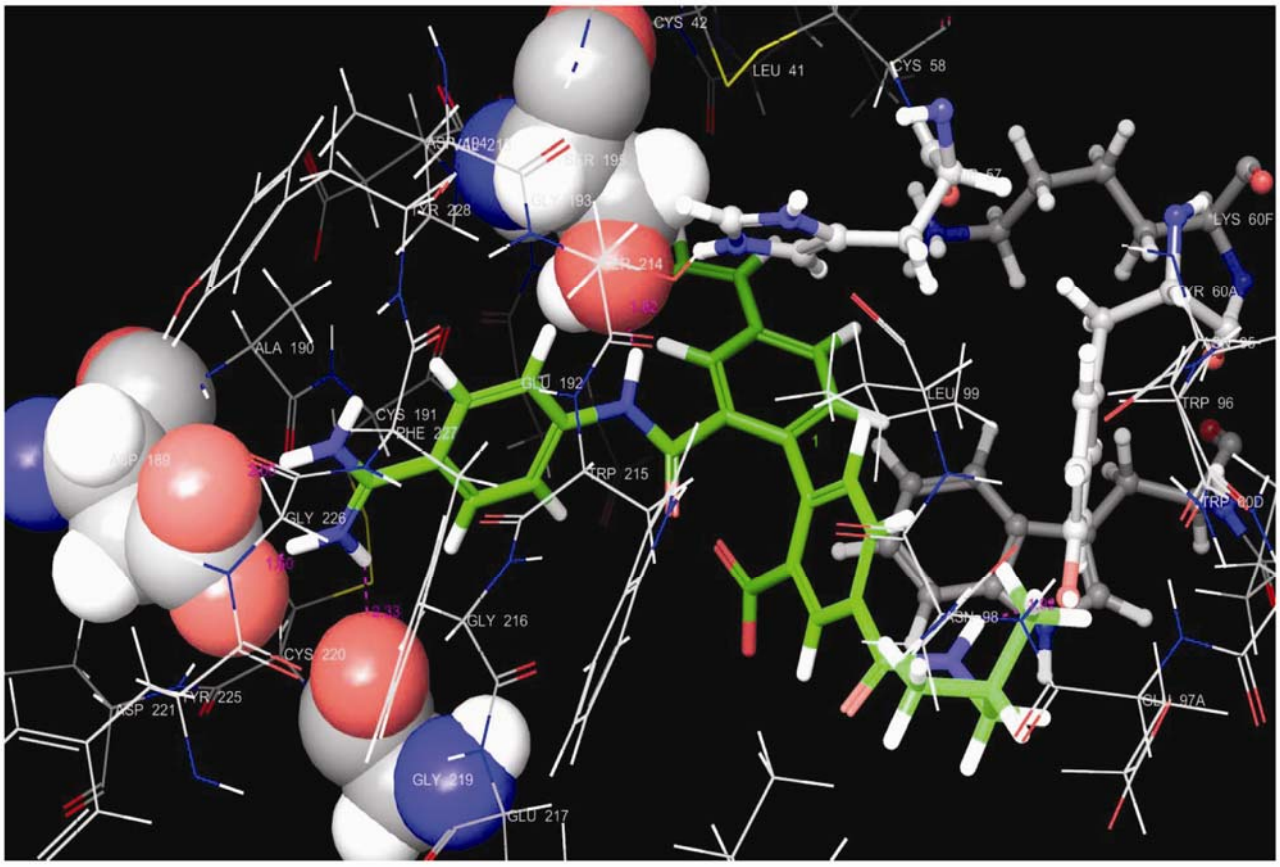

Figure 6. Glide XP docking of compound **4** (in green) into active site of thrombin; Hydrophobic interacting residues (in white); H-bond interacting residues (in CPK model).

activity. Visual analysis of Figure 5 *b* demonstrates the presence of hydrophobic interactions; wherein the blue region near the 4-position of the aromatic ring hypothesis (R12) shows presence of hydrophobic group. The aromatic ring is well accepted in the hydrophobic area, which means there is increase in biological activity due to this interaction; this phenomenon is well depicted in compounds such as **17**, **20** and **21**. These compounds contain various aromatic substituents at 4-position of the phenyl ring, which results into increase in biological activity. It is similar in compound **16**, as the presence of benzene ring at 4-position of the aromatic ring increases biological activity. Similarly, an increase in biological activity is seen for the reference compound **35** due to the presence of ethyl group in the 4-position of the aromatic ring, which indulges in strong bonding. In electron negative volume occlusion map (Figure 5 *c*) the red cubes at 4-position of the aromatic ring suggest that the presence of electronegative group decreases biological activity, as seen in compounds **27**, **29** and **30**. At physiological pH, compound **33** which contains azidomethyl group attached to 3-position of thiophene ring, gets protonated and acts as electron-withdrawing group from the aromatic ring (Figure 5 *d*). This results in increase in electron density in the azido group and so the biological activity of compound **33** falls in inactive pharmaset. In summary, presence of polar group at 4-position of aromatic ring (R12) results in decrease in biological activity, whereas presence of hydrophobic moiety at 4-position of aromatic hypothesis (R12) increases biological activity.

To validate common pharmacophoric features and 3D-QSAR model, docking studies of active pharmaset compounds were carried out with the 3D structure of human thrombin (PDB code: 2C8W). Docking scores of the 10 active compounds which were docked against thrombin are given in Table 3.

The resultant docking study was found to be complementary with pharmacophore as well as 3D-QSAR studies. Compound **4** predicted highest docking score, i.e. –9.658; thus it is an ideal candidate to study binding interactions with thrombin. Docking conformation of prototype compound **4** can be seen in Figure 6. The figure shows the interaction of compound **4** with the amino acids in the active site of thrombin. A hydrophobic pocket is formed by the amino acids such as TRP60D, TYR60A, LYS60F, LEU99, HIS57 and TRP215 surrounding the main biphenyl moiety. These amino acid residues contributing to hydrophobic interactions are highlighted in white colour. Hydrogen bonding between the ligands and the enzyme plays a vital role in stabilizing the ligand in

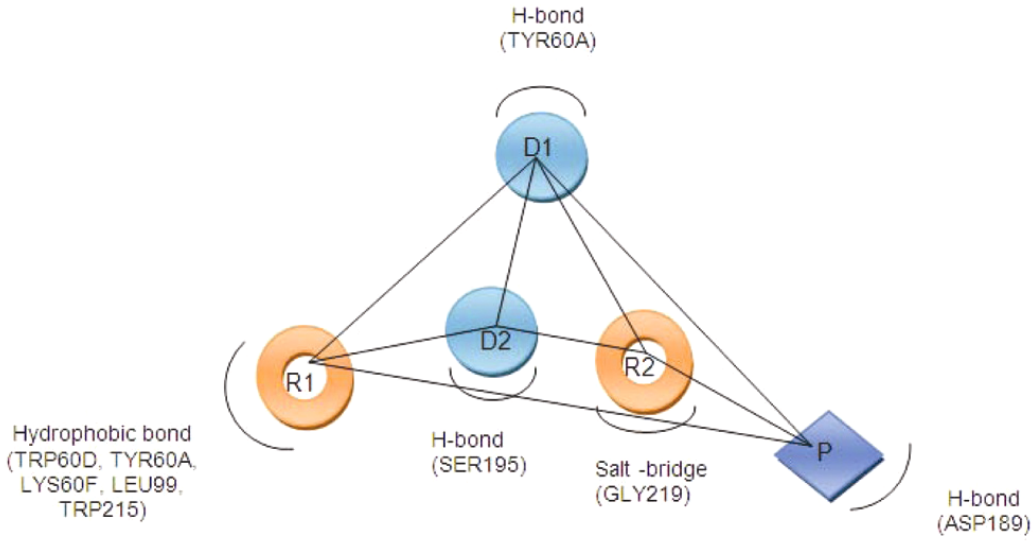

Figure 7. Representation of interaction between pharmacophore features and active site residues of thrombin.

the active site of thrombin. A network of dynamic hydrogen bond forms between the amino-methaniminium group and ASP 189 with distance ranging from 1.60 to 2.00 Å. Further, the two amide groups of benzamide and isobutylformamide act as hydrogen bond donors and form hydrogen bonds with SER195 (1.82 Å) and TYR60A (1.92 Å) respectively. The benzimidamide at physiological pH gets protonated to amino (phenyl)-methaniminium and forms a salt bridge with GLY219 (2.33 Å), which validates the generated pharmacophoric features. Similar docking configuration was adopted by other compounds in the active pharmaset, which are complementary to the generated pharmacophore. Figure 7 displays the pharmacophore features interacting with thrombin active site residues, which represents the interactions of active compounds.

The present work provides ligand-based pharmacophore modelling and 3D-QSAR studies of some potent biphenyl antithrombin compounds. The pharmacophore model illustrated two aromatic rings (R), two hydrogen donors (H) and one positive ionizable group (P) in biological activity. Structure–activity relationship amongst the molecules was visualized using 3D-QSAR model. Docking of these biphenyl compounds with crystal structure of thrombin revealed favourable hydrogen bond interactions. Biphenyl moiety of the active compound is well accepted in the hydrophobic pocket of the thrombin active site. This shows that biphenyl analogues can be ideal antithrombin drug candidates. The study carried out can be used as a valuable tool for the rational drug-design process, which provides precise attributes for the design of better analogues. Thus, the pharmacophore and atom-based 3D-QSAR model presented here could be useful for the development of new biphenyl leads as thrombin inhibitors.

1. Furie, B. and Furie, B. C., *In vivo* thrombus formation. *J. Thromb Haemostasis* (*Suppl. 1*), 2007, **5**, 12–17.
2. Davie, E. W. *et al*., The coagulation cascade: initiation, maintenance, and regulation. *Biochemistry*, 1991, **30**, 10363–10370.
3. Stormorken, H., The discovery of factor V: a tricky clotting factor. *J. Thromb. Haemostasis*, 2003, **1**(2), 206–213.
4. Antonarakis, S. E., Molecular genetics of coagulation factor VIII gene and hemophilia A. *J. Thromb. Haemostasis*, 1995, **74**(1), 322–328.
5. Walsh, P. N., Roles of platelets and factor XI in the initiation of blood coagulation by thrombin. *J. Thromb. Haemostasis*, 2001, **86**(1), 75–82.
6. Charles, S., Greenberg, C. S. and Shuman, M. A., Specific binding of blood coagulation factor XIII, to thrombin stimulated platelets. *J. Biol. Chem.*, 1984, **259**(23), 14721–14727.
7. Kini, R. M., Toxins in thrombosis and haemostasis: potential beyond imagination. *J. Thromb. Haemostasis.* (*Suppl. 1*), 2011, **9**, 195–208.
8. Hirsh, J. *et al.*, Oral anticoagulants: mechanism of action, clinical effectiveness, and optimal therapeutic range. *Chest* (*Suppl. 1*), 2001, **119**, 8S–21S.
9. Hirsh, J. *et al*., Heparin and low-molecular-weight heparin: mechanisms of action, pharmacokinetics, dosing, monitoring, efficacy, and safety. *Chest* (*Suppl. 1*), 2001, **119**, 64S–94S.
10. Bauer, K. A., Hawkins, D. W., Peters, P. C., Petitou, M., Herbert, J. M., van Boeckel, C. A. and Meuleman, D. G., Fondaparinux, a synthetic pentasaccharide: the first in a new class of antithrombotic agents – the selective factor Xa inhibitors. *Cardiovasc. Drug Rev*., 2002, **20**(1), 37–52.
11. Stubbs, M. T. and Bode, W., The clot thickens: clues provided by thrombin structure. *Trends Biochem. Sci.*, 1995, **20**(1), 23–28.
12. Bode, W., The structure of thrombin: a janus-headed proteinase. *Semin. Thromb. Hemostasis*, 2006, **32**, 16–31.
13. Di Cera, E., Thrombin. *Mol. Aspects Med.*, 2008, **29**(4), 203–254.
14. Yasuo, K., Feng, N., Torsten, S. and John, D., Thrombin inhibitors based on the amino acid sequence of hirudin. The National Research Council of Canada, Patent number US6060451, 9 May 2000.
15. Bartel, S., Hahn, M. G. and Moradi, W., Biphenyl compounds useful in the treatment or prevention of cardiovascular disorders. Bayer Schering Pharma Aktiengellschaft, Patent number US7998988, August 2011.

16. Nageswar, R. C. *et al.*, Synthesis and antithrombotic activity study of some new thienopyridine derivatives. *Lett. Org. Chem.*, 2011, **8**(6), 412–415.
17. Nageswar, R. C., Mamidisetty, B., Mahesh, R. G. and Padi, P. R., Synthesis and pharmacological evaluation of 5-[2′-(1H-tetrazol-5-yl)-biphenyl-4-ylmethyl]-4,5,6,7-tetrahydro-thieno[3,2-c]pyridine derivatives as platelet aggregation inhibitors. *J. Saudi Chem. Soc*., 2011, DOI: 10.1016/j.jscs.2011.10.016.
18. Lacefield, *et al*., Arylacetylene compounds as antithrombotic agents. Eli Lilly and Company, Patent number US 3968251, July 1976.
19. Kotian, P. L. *et al*., Design, parallel synthesis, and crystal structures of biphenyl antithrombotics as selective inhibitors of tissue factor FVIIa complex. Part 1: Exploration of S2 pocket pharmacophores. *Bioorg. Med. Chem*., 2009, **17**, 3934–3958.
20. Mahipal, T. O. P., Karthikeyan, C., Moorthy, N. S. and Trivedi, P., 3D QSAR of aminophenyl benzamide derivatives as histone deacetylase inhibitors. *Med. Chem*., 2010, **6**, 277–285.
21. Dixon, S. L., Smondyrev, A. M. and Rao, S., PHASE: A novel approach to pharmacophore modeling and 3D database searching. *Chem. Biol. Drug Des.*, 2006, **67**, 370–372.
22. Dixon, S. L., Smondyrev, A. M., Knoll, E. H., Rao, S. N., Shaw, D. E. and Friesner, R. A., PHASE: a new engine for pharmacophore perception, 3D QSAR model development, and 3D database screening: 1. Methodology and preliminary results. *J. Comput. Aided Mol. Des.*, 2006, **20**, 647–671.
23. Kolossvary, I. and Guida, W. C., Low mode search: an efficient, automated computational method for conformational analysis application to cyclic and acyclic alkanes and cyclic peptides. *J. Am. Chem. Soc*., 1996, **118**, 5011–5019.
24. Shelke, S. M., Bhosale, S. H., Dash, R. C., Suryawanshi, M. R. and Mahadik, K. R., Exploration of new scaffolds as potential MAO-A inhibitors using pharmacophore and 3D-QSAR based *in silico* screening. *Bioorg. Med. Chem. Lett.*, 2011, **21**, 2419–2424.
25. Golbraikh, A., Shen, M., Xiao, Z., Xiao, Y. D., Lee, K. H. and Tropsha, A., Rational selection of training and test sets for the development of validated QSAR models. *J. Comput. Aided Mol. Des*., 2003, **17**, 241–253.
26. Friesner, R. A. *et al.*, Glide: a new approach for rapid, accurate docking and scoring. 1. Method and assessment of docking accuracy. *J. Med. Chem.*, 2004, **47**, 1739–1749.
27. Friesner, R. A. *et al.*, Extra precision glide: docking and scoring incorporating a model of hydrophobic enclosure for protein–ligand complexes. *J. Med. Chem.*, 2006, **49**, 6177–6196.
28. Schrödinger Suite 2009 Protein Preparation Wizard; Epik version 2.0; Impact version 5.5. Schrödinger, LLC, New York.

ACKNOWLEDGEMENTS. A.N.J. thanks the Council of Scientific and Industrial Research – Unit for Research and Development of Information Products, Pune for providing financial support. We also thank the Centre for Development of Advanced Computing, Bioinformatics Resource and Application Facility, Pune, for providing computational facility.

Received 28 February 2013; revised accepted 3 September 2013

Detection and size distribution analysis of ice floes near Antarctica using RISAT-1 imagery

S. Srisudha, A. Senthil Kumar*, D. S. Jain and V. K. Dadhwal

National Remote Sensing Center (ISRO), Balanagar, Hyderabad 500 625, India

This study shows that C-band FRS-1 image mode data from RISAT-1 mission can be exploited to identify and monitor ice floes in the polar regions. The ice floes size distribution plays a vital role in understanding both ice motion dynamics and polar species habitat in the sea-ice zones. An automated algorithm was chosen here as against manual approach for identification of the floes for operational ice-floe mapping. The assessment of mapping accuracy was estimated to be about 80%. This exercise may help initiate temporal variations of the ice-floe size distribution to support ice-floe formation processes and climatic impact studies.

Keywords: Ice-floe detection, polar sea-ice, radar imagery, size distribution analysis.

ICE floes result from fracturing of thick sea-ice in the polar regions largely due to strong winds and waves that prevail in these regions seasonally. These ice floes have different shapes and sizes ranging from about a metre to a few kilometres. The size distribution of these floes has become an important model parameter in the dynamic and thermodynamic processes of sea-ice area. The melting rate of ice floes, for example, depends on the ice-floe size; smaller the ice floes higher is the lateral melting[1]. Also, it was shown that momentum transferred from the atmosphere to ice would vary with the ice-floe size[2]. The size distribution and shape of ice floes would provide a clue to the understanding of ice-floe formation processes[3,4]. Besides, such analyses provide a lead to ice motion tracking as a part of warning alerts of ship routing. Also, polar species like walrus are attracted to ice floes that can support their weight; the ice-floe size distribution is necessary to determine the links between species habitat and sea-ice[5].

Though many research studies based on sea truth survey expeditions have been carried out routinely for ice-floe monitoring, space-borne remotely sensed data analysis stands undisputed as the only means of operationally monitoring ice-floe motion analysis by virtue of its unique advantages of larger coverage and high repeat cycle capabilities of the present-day on-board sensors. The sensors operating in the microwave region of the electromagnetic spectrum are better suited than their

*For correspondence. (e-mail: senthilkumar_a@nrsc.gov.in)